Phonons in the icosahedral quasicrystal *i*-AlPdMn studied by inelastic x-ray scattering

M. Krisch

European Synchrotron Radiation Facility, F-38043 Grenoble Cedex, France

R. A. Brand*

Department of Physics, Gerhard-Mercator-Universität Duisburg, D-47048 Duisburg, Germany

M. Chernikov

Center for Superconductivity at the University of Houston, Houston, Texas 77204-5932

H. R. Ott

Laboratorium für Festkörperphysik, Eidgenössische Technische Hochschule-Hönggerberg, CH-8093 Zürich, Switzerland

The phonon branches of a *i*-AlPdMn icosahedral quasicrystal are studied, using inelastic x-ray scattering (IXS) with meV energy resolution. Longitudinal and transverse phonon branches are recorded, starting from a (52,84) reflection along the twofold axis. In both cases we observe an acoustic mode whose speed of sound agrees very well with the sound velocity at small reduced wave vectors q, but becomes nondispersive near $q \sim 0.35$ Å^{-1}. A second mode, dispersionless over the whole spanned q range, can be clearly identified only in a purely longitudinal geometry. Our findings are in general agreement with previous inelastic neutron scattering (INS) results. However, at variance with the INS results, we observe a weaker increase of the longitudinal acoustic phonon line width with reduced momentum transfer. The present study presents a benchmark for future IXS work on quasicrystalline materials which will be of particular value for single crystals, only available in very small quantities or containing elements not suitable for INS due to their large incoherent cross section.

I. INTRODUCTION

Quasicrystals constitute a class of solids different from both crystals and glasses, since at the same time they show sharp diffraction peaks and a point-group symmetry that is incompatible with lattice periodicity.[1] Their thermal and vibrational properties have remained difficult to understand. It has long been noted that low-temperature specific-heat measurements[2] do not agree with the experimental sound velocity[3] and vibrational density of states.[4] In these early works, the weak sample-dependent magnetism of Mn led to much of the confusion. In the case of diamagnetic *i*-AlCuFe, Brand *et al.*[5] have shown the quantitative agreement between the measured lattice specific heat and that predicted from the measured density of states (DOS). In this case, the low-energy region is strongly non-Debye-like, indicating the presence of localized vibrational states. Thus it is of paramount interest not only to measure the vibrational DOS, but as well the individual phonon branches themselves. Therefore, coherent inelastic neutron scattering (INS) has been extensively used to study the phonon dispersion relations in the icosahedral quasicrystals *i*-AlPdMn,[6–8] *i*-AlLiCu,[9,10] and *i*-AlCuFe,[11,12] as well as decagonal *d*-AlNiCo.[13] Well-defined acoustic phonon modes with instrumental linewidths are found close to strong Bragg reflections. They show a linear dispersion up to a reduced wave vector of about 4 nm^{-1}. Above this, these excitations broaden out into a dispersionless band. In addition, another branch, not seemingly connected with any reflection, is observed higher in energy than the plateau of the acoustic branch, and is conventionally denoted the optical branch. Finally, additional dispersionless modes have been identified, and partly associated with crossing with quasi-Brillouin-zone boundaries.[7]

In the present work we study the phonon spectrum of the well-known quasicrystal system *i*-AlPdMn, utilizing inelastic x-ray scattering (IXS) with meV energy resolution. This technique has been rapidly evolving in the past 15 years, following pioneering experiments[14,15] (see Ref. 16 for a recent review), and made important contributions in the study of the high-frequency dynamics of disordered matter in the regime of small momentum transfer and large energy transfer, which is very difficult to access by INS due to kinematic limitations (see, for example, Refs. 17 and 18). For single crystals the advantage of IXS arises from the availability of intense, highly collimated x-ray beams, generated by undulator sources, and high-performance x-ray optics, which allow one to routinely obtain spot sizes of the order of tens of microns. This, in turn, permits us to study samples available only in small quantities, which would not yield sufficient signals to perform an INS experiment. As a starting point for quasicrystal work, we have chosen the well-studied *i*-AlPdMn system, because phonon dispersion data do exist so that a comparison with previous results can be made. Our goal is to show that IXS is capable of yielding reliable information on the phonon dispersion for small single-grain quasicrystals, therefore opening up the possibility of studying systems for which only single-grain samples as small as 10^{-3} mm^3 are available; and more generally, to provide further insight into the dynamics of these exotic materials.

II. INELASTIC X-RAY CROSS SECTION

In order to underline the similarities and differences between coherent inelastic x-ray and neutron scattering, we briefly outline the formalism for one-phonon scattering in single crystals. IXS probes the dynamic structure factor associated with the collective motions of the atoms (molecules) within the validity of the following assumptions:[19–21] (i) The scattering process is dominated by the Thomson scattering term, and the other resonant and spin-dependent contributions to the electron-photon scattering cross section can be neglected at the considered energy transfers. (ii) The adiabatic approximation allows one to separate the electronic and nuclear parts of the total wave function, and therefore the center of mass of the electronic cloud follows the nuclear motion. (iii) There are no electronic excitations in the considered energy transfer range. Under the above conditions, the IXS double differential cross section can be written as[19]

$$\frac{\partial^2\sigma(E,\Omega)}{\partial\Omega\,\partial E}=r_0^2(\vec{\varepsilon}_i\cdot\vec{\varepsilon}_f)^2\frac{k_f}{k_i}S(E,\vec{Q}),\qquad(1)$$

where E and $\vec{Q}$ are the energy and momentum transfer to the scattering system. Ω denotes the solid angle in which the inelastic scattered x rays are observed; r_0 is the classical electron radius; $\vec{\varepsilon}_i$ and $\vec{\varepsilon}_f$ are the photon polarization vectors of the incident and scattered photons, and k_i and k_f are their respective wave vectors (in contrast to INS, for IXS $k_i\approx k_f$). $S(E,\vec{Q})$ denotes the dynamical structure factor, which reflects the properties of the scattering system in the absence of the perturbing probe. The prefactor to $S(E,\vec{Q})$ is the Thomson scattering cross section, describing the coupling to the electromagnetic field. For a periodic structure with n atoms in the unit cell the response function is a sum over the $3n$ normal modes of the system:

$$S(E,\vec{Q})=\sum_j S_j(E,\vec{Q}).\qquad(2)$$

Here j is the label of a specific phonon branch. For each branch the phonon wave vector is given by $\vec{q}=\vec{Q}-\vec{G}$, where $\vec{G}$ is the closest reciprocal-lattice vector. In the harmonic approximation, the dynamical structure factor is given by[16]

$$S_j(E,\vec{Q})=\left(\frac{1}{1-\exp\left(-\dfrac{E}{k_BT}\right)}\right)\frac{F_{in}(\vec{Q})}{E_j(\vec{q})}$$

$$\times\delta[E\mp E_j(\vec{q})].\qquad(3)$$

The first term is the detailed balance factor, D, that describes the phonon population at temperature T; k_B is the Boltzmann constant. The delta function involving a difference (sum) corresponds to phonon creation (annihilation). The inelastic structure factor $F_{in}(\vec{Q})$ is obtained by summing over all atoms in the unit cell:
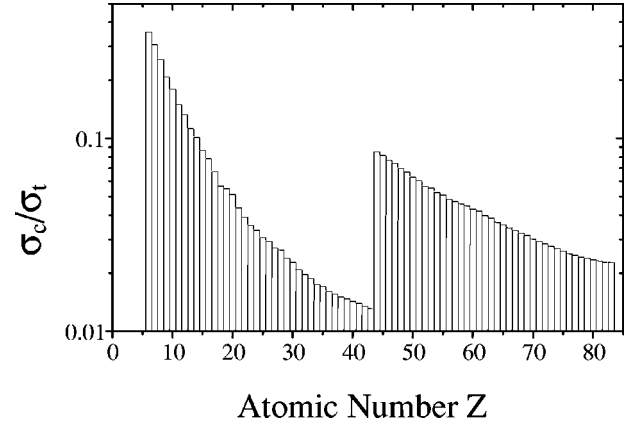

FIG. 1. Ratio between coherent σ_c and the total scattering cross section σ_t for x rays of incident energy 22 keV vs atomic number (from Ref. 22).

$$F_{in}(\vec{Q})=\left|\sum_k M_k^{-1/2}f_k(\vec{Q})[e_k^j(\vec{q})\cdot\vec{Q}]\exp(i\vec{Q}\cdot\vec{r}_k)\right.$$

$$\left.\times\exp(-W_k)\right|^2.\qquad(4)$$

Here M_k is the mass, $f_k(\vec{Q})$ is the atomic form factor, $\exp(-W_k)$ is the Debye-Waller factor, and $\vec{r}_k$ is the position of atom k in the unit cell. $e_k^j(\vec{q})$ denotes the phonon eigenvector with wave vector $\vec{q}$ of atom k in mode j. With respect to the INS cross section we note the following differences.

(i) The IXS $S(E,\vec{Q})$ is proportional to $f_k^2(\vec{Q})$. For $\vec{Q}\rightarrow 0$, then $f_k(\vec{Q})\rightarrow Z$, whereas for large $\vec{Q}$ the atomic form factor decreases. For INS, $f_k(\vec{Q})$ has to be replaced by the scattering length b_k, which is independent of $\vec{Q}$, and its magnitude does not follow any systematic function of the atomic number.

(ii) The IXS cross section is purely coherent, whereas the cross section for neutrons possesses an element-dependent incoherent contribution.

(iii) At the considered x-ray energies, the photoelectric absorption process is the main process alternative to the Thomson scattering. Photoelectric absorption has a cross section increasing roughly with the atomic number Z as Z^4, and therefore is the determining factor for the sample scattering volume.

To further illustrate the above points, in Fig. 1 we display the Z dependence of the efficiency of the IXS method with a typical incident photon energy of 22 keV.[22] This can be expressed by the ratio between the number of photons scattered by the Thomson process, and the number of photons absorbed by the system through all other scattering processes. As a matter of fact, this quantity is nothing else than the ratio σ_c and σ_t, where $\sigma_t=\mu/\rho$ and σ_c are the total and coherent cross sections per atom. The step between $Z=44$ and 45 signifies the energy of the K-shell absorption edge with respect to the incident photon energy. If the photon energy is smaller than the K-shell binding energy more sample can be
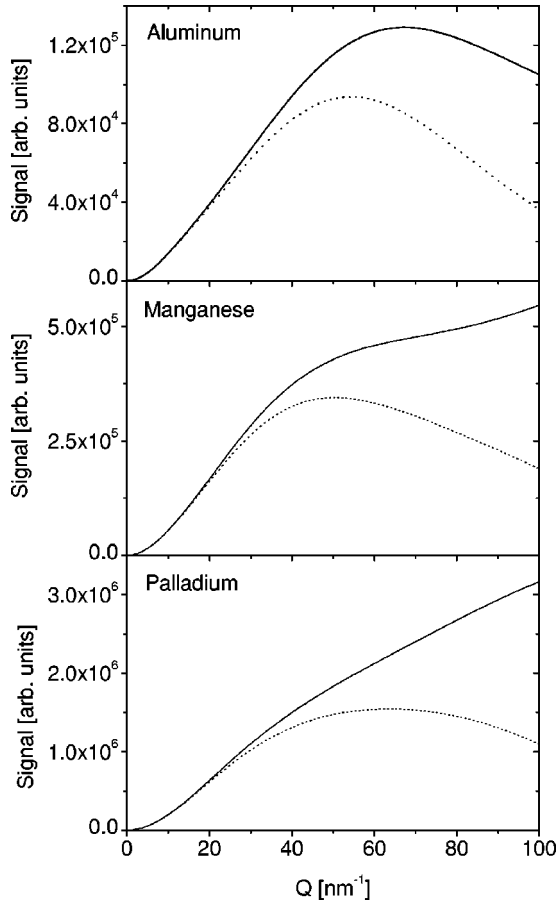
FIG. 2. The product $[f(Q)Q]^2$ (solid line) and $(f(Q)Q)^2\cos^2(\theta_s)$ (dotted line)] as a function of momentum transfer Q at 22 keV.

probed, whereas in the other case another absorption channel opens up, and consequently the scattering volume is reduced.

Inspection of Eqs. (1) and (4) shows that the IXS cross section is proportional to $f_k^2(Q)Q^2(\vec{\varepsilon}_i\cdot\vec{\varepsilon}_f)^2$. For x rays which are linearly polarized in the horizontal plane, and scattering in the horizontal plane, $(\vec{\varepsilon}_i\cdot\vec{\varepsilon}_f)^2=\cos^2(\theta_s)$, where θ_s is the scattering angle. This proportionality is displayed in Fig. 2 for the three constituent elements of the quasicrystal, namely, aluminum, manganese, and palladium. The solid curve of each graph shows only the factor $f_k^2(Q)Q^2$, whereas in the dotted curve the polarization factor is included. While for the lightest element the drop in the atomic form factor is not compensated for by the Q^2 term, this is no longer true for the two heavier elements constituting the quasicrystal, where the Q^2 dependence becomes dominant. However, the polarization term ultimately leads to a dependence in Z with a maximum located between 50 and 60 nm^{-1}. The range in which the IXS experiment was performed (40–50 nm^{-1}) is therefore close to the optimum value, and where the palladium atoms yield the strongest contribution to the signal. More specifically, assuming Al$_{68.2}$Pd$_{22.8}$Mn$_9$ and a typical Q value of 48 nm^{-1}, the contribution to the signal from Al, Mn, and Pd for IXS amounts to 14.7, 7.3, and 78%, respectively. In contrast to this, an analogous analysis for INS yields that the signal from Al and Pd have almost identical strengths.

It is evident that the formalism described above, is appropriate for phonons in single crystals, and cannot be simply transferred to the case of quasicrystals. The absence of three-dimensional periodicity leads to an infinitely large unit cell, and consequently, no Brillouin zone can be defined. On the other hand, very strong and narrow Bragg peaks can be observed, which can be utilized to define pseudo-Brillouin-zones with Bragg positions as zone centers.[6] Moreover, in the long-wavelength limit, the phonons do not sense the spatial nonperiodicity, and sound waves are expected to propagate as in a continuum medium. Regarding the structure and the dynamics, quasicrystals are therefore located in between the perfect single crystal on one side, and the amorphous solid on the other hand.

III. EXPERIMENTAL DETAILS

The experiment was carried out at the Inelastic X-ray Scattering Beamline II (ID28) at the European Synchrotron Radiation Facility in Grenoble/France. The x-ray beam from the third harmonics of a 35-mm period linear undulator was premonochromatized to $\Delta E/E=2\times10^{-4}$ by a cryogenically cooled silicon (1 1 1) double-crystal monochromator. This energy resolution of the photons is further improved by the high-energy resolution backscattering monochromator.[23] It consists of a flat, symmetrically cut silicon crystal oriented along the (1 1 1) direction, operating at a Bragg angle of 89.98°, and temperature controlled with a precision of 0.2 mK over the 285–295-K temperature region. The family of crystalline planes used by the monochromator has to be chosen as a compromise between the energy resolution and incident photon flux on the sample. In the present experiment we chose to work with Si (9 9 9) and the Si (11 11 11) reflection orders, providing energy resolutions of 2.0 and 1.0 meV, respectively. The backscattered beam impinges on a gold-coated toroidal mirror, which provides a focal spot at sample positions of 270-μm (horizontal) and 80 μm (vertical). The scattered photons are energy analyzed by a 6.5-m Rowland circle crystal spectrometer, operating at the same reflection order and the same Bragg angle as the high-resolution monochromator.[24,25] A Peltier-cooled silicon diode detector with an intrinsic energy resolution of 400 eV (Ref. 26) detects the energy-analyzed photons. The dark counts due to electronic and environmental noise amounts to about 0.2 counts/minute. The analyzer crystal is temperature stabilized at about 22.5 °C with a typical stability of 1 mK/24 h. The momentum transfer $Q=2k_{in}\sin(\theta_s/2)$ is selected by rotating the spectrometer arm around a vertical axis passing through the sample in the horizontal plane. The momentum-transfer resolution is defined by motorized slits in front of the crystal analyzer, and its standard setting yields $\Delta Q=\pm0.13$ nm^{-1} [at Si (9 9 9)] and ±0.165 nm^{-1} [at Si (11 11 11)]. The energy scans are performed by varying the monochromator temperature while the analyzer temperature is kept fixed. Conversion from the temperature scale to the energy scale is accomplished by the following relation: $\Delta E/E=\alpha\Delta T$, where $\alpha=2.58\times10^{-6}$ is the linear thermal expansion of silicon around room temperature. The validity of this conversion has been verified by comparing the measured diamond
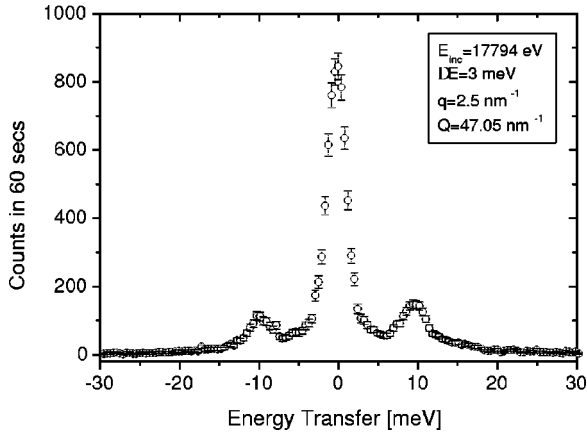
FIG. 3. Typical IXS scan obtained under conditions as indicated in the graph.

dispersion curve for longitudinal acoustic phonons with well-established inelastic neutron-scattering results. The overall experimental resolution is determined by measuring the scattering from a disordered sample of plexiglass at a Q transfer of 10 nm^{-1}, corresponding to the first maximum in the static structure factor $S(Q)$, and at $T=10$ K in order to maximize the elastic contribution to the scattering.

The sample was a single-grain of the icosahedral quasicrystal i-AlPdMn. It was cut with a twofold axis perpendicular to the surface. The measured mosaic spread was 0.03°. The (52,84) reflection was chosen as it lies conveniently on a twofold axis, and is the strongest reflection at this large vector G. We denote the deviation from this reflection as $q = Q - G$. We have studied both the longitudinal acoustic (LA) mode along the twofold direction as well as the transverse acoustic (TA) mode perpendicular to the twofold axis up to $q=5$ nm^{-1}. The sample was mounted in reflection geometry.

IV. EXPERIMENTAL RESULTS

A typical IXS spectrum, recorded at $Q = 47.05$ nm^{-1} ($q=2.5$ nm^{-1}) in longitudinal geometry close to the 52/84 reflection, is displayed in Fig. 3, where the normalized intensity in counts per minute is plotted versus the energy transfer. The spectrum consists of an elastic line at zero energy, whose width is, in analogy to glasses, resolution limited, and a clearly visible Brillouin doublet, constituting the phonon gain and phonon loss peaks.

Figure 4 shows the complete set of data recorded with an energy resolution of 3 meV along the twofold axis in longitudinal geometry. In a first step, a Lorentzian line shape and a damped harmonic oscillator (DHO) mode, both with a single excitation, were used to fit the data. Neither model led to satisfactory agreement, reflected in a fairly high χ^2 value. This is not surprising, since in all spectra at least one additional spectral feature is clearly visible. Therefore, guided by the analysis performed for the coherent inelastic neutron scattering experiments,[5,6] the IXS spectral shape was fitted by two pairs of damped harmonic oscillators for the inelastic features and a Lorentzian line for the elastic peak. This
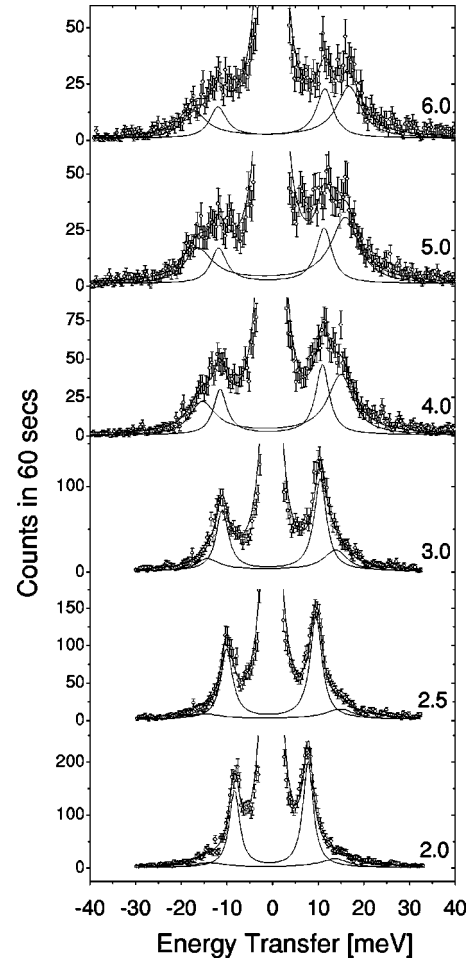

FIG. 4. IXS scans obtained with an energy resolution of $\Delta E = 3$ meV in longitudinal geometry and at q values indicated in the graph. The experimental data, displayed with their error bars, are shown together with the best fit to a model function as explained in the text. The total fit as well as its individual inelastic parts are shown.

model function is convoluted with the experimentally determined resolution function, and the fitting procedure is performed using standard χ^2-minimization routines. All the fits yield a χ^2 value around 1, thus testifying to the quality and reliability of the fit.

In order to extend the spanned Q range to lower Q values and to provide evidence of the predicted additional inelastic features at small energy transfers, spectra were recorded with an improved energy resolution of 1.5 meV [Si (11 11 11) reflection order at 21747 eV), both in longitudinal and transverse geometries. These spectra are shown in Figs. 5 and 6. The data in longitudinal geometry confirm the existence of two distinct modes, and moreover provide evidence for additional features at around 4 meV (spectra at 1.5 and 2.0 nm^{-1}). It has to be stressed, however, that their existence can be only deduced from the incapability of the model function to fit the data. The spectra taken in transverse geometry are of poorer statistical quality due to the lower count time per point, but within the statistical quality of the data, a
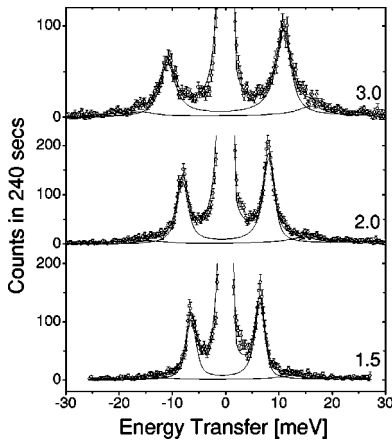
FIG. 5. IXS scans obtained with an energy resolution of ΔE = 1.5 meV in longitudinal geometry and at q values indicated in the graph. The experimental data, displayed with their error bars, are shown together with the best fit to a model function as explained in the text. The total fit as well as its individual inelastic parts are shown.

model function consisting of only one pair of DHO well reproduces the main features of the data.

The top panel of Fig. 7 shows the resulting dispersion curves for longitudinal phonons. The IXS data are displayed together with the INS results. Moreover, the sound speed in the long wavelength limit, as obtained by ultrasonic measurements[3] is shown by the solid line. The longitudinal dynamics is characterized by two main excitations (exclud-
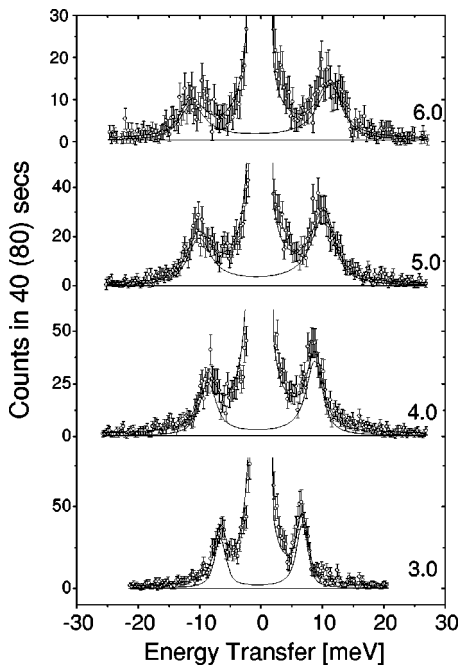

FIG. 6. IXS scans obtained with an energy resolution of ΔE = 1.5 meV in transverse geometry and at q values indicated in the graph. The experimental data, displayed with their error bars, are shown together with the best fit to a model function as explained in the text. The total fit as well as its individual inelastic parts are shown.
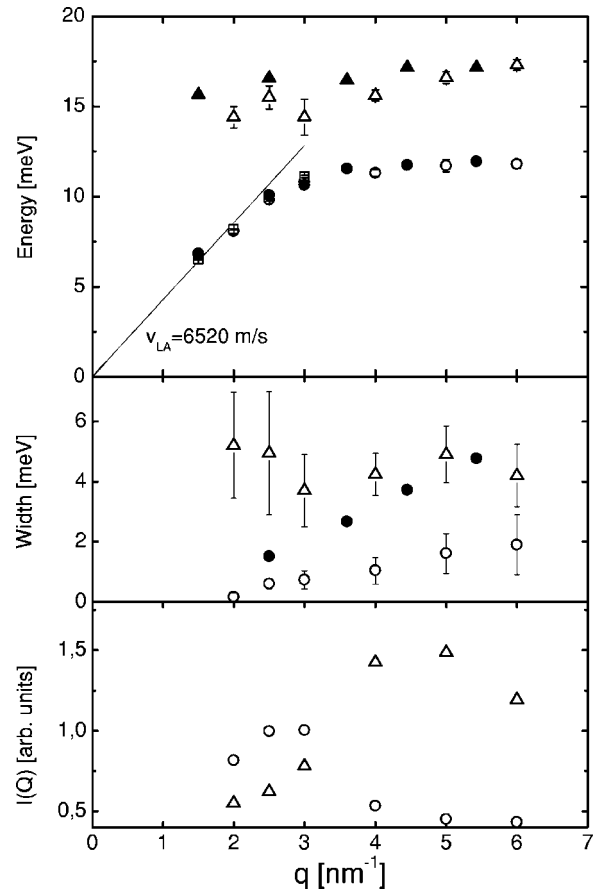

FIG. 7. Top: dispersion curve of the longitudinal dynamics. Middle: phonon widths of the two identified branches. Bottom: phonon intensities $I(Q)$, corrected for the detailed balance factor (DBF), the phonon energy E, and the momentum transfer Q (see the text). Open circles (IXS, LA branch, $\Delta E = 3$ meV); open squares (IXS, LA branch, $\Delta E = 1.5$ meV); open triangles (IXS, LO branch, $\Delta E = 3.0$ meV); full circles (INS, LA branch, $\Delta E = 1.3$ meV); full triangles (INS, LO branch, $\Delta E = 1.3$ meV); solid line (speed of sound as determined by ultrasonic measurements).

ing further excitations for the moment), one which can, due to its dispersive character, be assigned to a LA mode, and the second one to an opticlike mode, which is visible in all the spectra, but shows only weak dispersion. The LA-phonon energy at the lowest q value measured results in a deduced speed of sound which is in good agreement with the ultrasonic measurements, whereas already from $q = 2$ nm^{-1} on, the LA branch starts to bend down and to flatten out for $q > 3$ nm^{-1}. The agreement between IXS and INS data for the LA branch is excellent, whereas for the LO branch the IXS data tend to lie slightly below the INS results. We do not consider this to be significant in view of the limited statistical quality of the data and the weak strength of the excitation at low momentum transfers. The middle panel shows the phonon widths as a function of momentum transfer. The LA widths show a clear q dependence, with an almost unbroadened phonon width at the lowest recorded q value of 2.0 nm^{-1}, whereas the LO branch shows within the error bars a q-independent broadening of about $4-5$ meV. The size of the error bars for the phonon widths are fairly large, re-
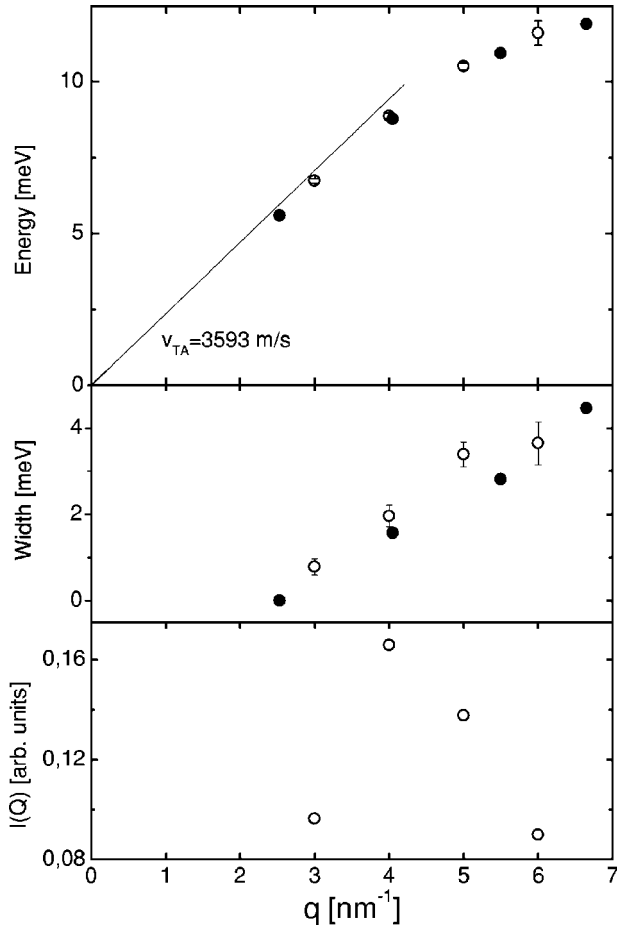
FIG. 8. Top: dispersion curve of the transverse dynamics. Middle: phonon widths of the TA branch. Bottom: phonon intensities $I(Q)$, corrected for the detailed balance factor (DBF), the phonon energy E, and the momentum transfer Q (see the text). Open circles (IXS, LA branch, $\Delta E = 1.5$ meV); full circles (INS, LA branch, $\Delta E = 1.3$ meV); solid line (speed of sound as determined by ultrasonic measurements).

flecting the difficulty to separate two closely lying excitations unambiguously. The LA-phonon widths, as determined by INS,[6,27] lie above the IXS ones. In general, the IXS Q resolution is better than the one for INS; moreover, it is energy and momentum transfer independent. Consequently, the discrepancy might be attributed to the orientation and size of the four-dimensional INS resolution function. The lowest panel of Fig. 7 shows the q dependence of the phonon intensities. These were obtained by integrating the fitted phonon profile for $E > 0$ and multiplying this value by $D^{-1}E_jQ^{-2}$, where D designs the detailed balance factor defined in Eq. (3). The value for the intensity thus obtained is proportional to the inelastic structure factor F_{in}, and should yield, at least in the small-q limit, an almost constant value.[28] This is approximately fulfilled for $q < 3$ nm^{-1}. For higher q values, the LA phonon loses intensity, and the LO intensity becomes dominant.

Figure 8 displays the results for the transverse dynamics. The phonon dispersion, reported in the top panel, is, as for the longitudinal dynamics, in very good agreement with INS

results. The phonon energy at the lowest q value of 3 nm^{-1} already deviates from the ultrasonic measurements. The q dependence of the IXS and INS phonon widths $\Gamma(q)$ are in good agreement, in contrast to the results for the longitudinal dynamics where the INS phonon widths were significantly higher. Focusing on the IXS results, the $\Gamma(q)$ dependence appears to be more pronounced for the TA branch than for the LA branch. This might be partly due to the fact that for the longitudinal dynamics a model function consisting of two DHO's was utilized. The statistical quality of the data, and the small energy separation between the two excitations, leads to a strong correlation of their respective widths. Moreover, the probable existence of further excitations, as inferred by INS measurements, makes a reliable determination of the momentum-transfer evolution of the phonon excitation width even more difficult.

V. CONCLUSIONS

Our results show the interest in coherent inelastic x-ray scattering as applied to the study of the phonon dispersion curves in quasicrystals. We summarize the main conclusions below.

(1) The IXS experiment confirms previous coherent inelastic neutron-scattering results as for the extrapolation to the speed of sound at small reduced scattering vector q and the overall shape of the dispersion curves.

(2) As in the case of INS, for the longitudinal dynamics we observe two main excitations at a given q. The first possesses the characteristics of an acoustic mode, dispersing as a function of momentum transfer, while the second one is only weakly dispersing. It appears to be absent in the purely transverse scans, and therefore must be of predominant longitudinal character.

(3) There is in addition some evidence of further modes at energies below the acoustic and the ''optic''modes. This is given both by the fact that these are seen directly in some spectra (see, i.e., the spectra at 1.5 and 2.0 nm^{-1} in Fig. 5), and the fact that the two-mode damped harmonic oscillator fit does not completely model the data.

(4) The results for the linewidth increase with q seems to deviate from those for INS in the case of the LA branch. This might be attributed to the orientation of the four-dimensional INS resolution function with respect to the dispersion sheet. Both acoustic branches show a progressive increase of the linewidth with q. It is therefore tempting to speculate on an analogy to amorphous solids where an approximately q^2 dependence of the acoustic mode linewidth is observed.[17]

(5) An important advantage of IXS with respect to INS is the fact that crystals or quasicrystals as small as 10^{-3} mm^3 can be studied, therefore opening up the possibility to study, for example, i-MgZnY, where good single grain crystals are only available in small quantities. Another advantage is the possibility to study samples containing elements not suitable for neutron scattering.

(6) It should be mentioned that the IXS spectra for quasicrystals contain a rather strong elastic peak, not present or

much weaker in either INS spectra of similar samples, or in IXS spectra of crystals. This is due to the Lorentzian form of the IXS instrument function (with its stronger wings), as compared to the more Gaussian form for INS.

(7) Finally, it turned out that recording both the energy-loss and -gain sides of the IXS spectrum leads to more stringent fits to the data, since it allows one to impose the condition of detailed balance.

Further work shall focus on a detailed study of the evolution of the phonon linewidth by accumulating IXS spectra with very good statistics, and eventually an improved energy resolution of 0.9 meV, and the extension of the technique to other quasicrystal samples which cannot be studied by coherent inelastic neutron scattering.

*Email address: r.a.brand@uni-duisburg.de

[1] C. Janot, *Quasicrystals: A Primer* (Oxford University Press, Oxford, 1992).

[2] Ch. Wälti, E. Felder, M.A. Chernikov, H. R. Ott, M. de Boissieu, and C. Janot, Phys. Rev. B **57**, 10 504 (1998).

[3] Y. Amazit, M. de Boissieu, and A. Zarembovitch, Europhys. Lett. **20**, 703 (1992).

[4] J.-B. Suck, J. Non-Cryst. Solids **153&154**, 573 (1993).

[5] R. A. Brand, A.-J. Dianoux, and Y. Calvayrac, Phys. Rev. B **62**, 8849 (2000).

[6] M. de Boissieu, M. Boudard, H. Moudden, M. Quilichini, R. Bellissent, B. Hennion, R. Currat, A. Goldman, and C. Janot, J. Non-Cryst. Solids **153&154**, 552 (1993).

[7] M. de Boissieu, M. Boudard, R. Bellissent, M. Quilichini, B. Hennion, R. Currat, A. I. Goldman, and C. Janot, J. Phys.: Condens. Matter **5**, 4945 (1993).

[8] M. Boudard, M. de Boissieu, S. Kycia, A. I. Goldman, B. Hennion, R. Bellisent, M. Quilichini, R. Currat, and C. Janot, J. Phys.: Condens. Matter **7**, 7299 (1995).

[9] A. I. Goldman, C. Stassis, R. Bellissent, H. Moudden, N. Pyka, and F. W. Gayle, Phys. Rev. B **43**, 8763 (1991).

[10] A. I. Goldman, C. Stassis, M. de Boissieu, R. Currat, C. Janot, R. Bellissent, H. Moudden, and F. W. Gayle, Phys. Rev. B **45**, 10 280 (1992).

[11] M. Quilichini, G. Heger, B. Hennion, S. Lefebre, and A. Quivy, J. Phys. (Paris) **51**, 1785 (1990).

[12] M. Quilichini, B. Hennion, G. Heger, S. Lefebre, and A. Quivy, J. Phys. II **2**, 125 (1992).

[13] F. Dugain, M. de Boissieu, K. Shibata, R. Currat, T. J. Sato, A. R. Kortan, J. B. Suck, K. Hradil, F. Frey, and A. P. Tsai, Eur. Phys. J. B **7**, 513 (1999).

[14] B. Dorner, E. Burkel, and J. Peisl, Nucl. Instrum. Methods Phys. Res. A **246**, 450 (1986).

[15] B. Dorner, E. Burkel, T. Illini, and J. Peisl, Z. Phys. B: Condens. Matter **69**, 179 (1987).

[16] E. Burkel, Rep. Prog. Phys. **63**, 171 (2000).

[17] F. Sette, M. H. Krisch, C. Masciovecchio, G. Ruocco, and G. Monaco, Science **280**, 1550 (1998).

[18] G. Ruocco and F. Sette, J. Phys.: Condens. Matter **11**, R259 (1999).

[19] E. Burkel, *Inelastic Scattering of X-Rays With Very High Energy Resolution*, Springer Tracts in Modern Physics Vol. 125 (Springer-Verlag, Berlin, 1991).

[20] W. Schülke, in *Handbook on Synchrotron Radiation*, edited by G. Brown and D. E. Moncton (Elsevier, Amsterdam, 1991), Vol. 3.

[21] F. Sette, G. Ruocco, M. Krisch, C. Masciovecchio, and R. Verbeni, Phys. Scr. **T66**, 48 (1996).

[22] R. Verbeni, Ph. D. thesis, University of Grenoble, 1998.

[23] R. Verbeni, F. Sette, M. H. Krisch, U. Bergmann, B. Gorges, C. Halcoussis, K. Martel, C. Masciovecchio, J. F. Ribois, G. Ruocco, and H. Sinn, J. Synchrotron Radiat. **3**, 62 (1996).

[24] C. Masciovecchio, U. Bergmann, M. Krisch, G. Ruocco, F. Sette, and R. Verbeni, Nucl. Instrum. Methods Phys. Res. B **111**, 181 (1996).

[25] C. Masciovecchio, U. Bergmann, M. Krisch, G. Ruocco, F. Sette, and R. Verbeni, Nucl. Instrum. Methods Phys. Res. B **117**, 339 (1996).

[26] Eurisys Mesures, Lingolsheim BP 311, 67834 Tanneries Cedex, France.

[27] M. Quilichini and T. Janssen, Rev. Mod. Phys. **69**, 277 (1997).

[28] B. Dorner, *Coherent Inelastic Neutron Scattering in Lattice Dynamics* (Springer-Verlag, Berlin, 1982).